Rethinking Image Restoration for Object Detection

Anonymous Author(s)
Affiliation
Address
email

Overview

In the supplemental material, we first give the proof of Theorem 1 in Section 1. We then analyze the convergence rate of Algorithm 1 in Section 2. Then we attach more results of targeted attack results on test sets for YOLOv3 [14] and Faster-RCNN [15] in Section 3. We then qualitatively compare our method with conventional training on several more real-world samples from RTTS and ExDark in Section 4. In Section 5 the statistics of object detection datasets are provided.

1 Proof of Theorem

Proposition 1 *Let $f, g : U \to \mathbb{R}$ be convex functions in a domain $U \subset \mathbb{R}^d$. We have two optimization problems with coefficients $s > 0$ and $\beta > 0$*

$$\min_{\mathbf{x}\in U} f(\mathbf{x}) \text{ s.t. } g(\mathbf{x}) \leq s, \tag{1}$$

$$\min_{\mathbf{x}\in U} f(\mathbf{x}) + \beta g(\mathbf{x}). \tag{2}$$

We assume that some constraint qualification such as Slater Condition is satisfied for (1). Strong duality thus holds for the above problem. Then for any $\beta > 0$, there exist $s > 0$ and vice versa, such that optimization problems (1) and (2) are equivalent.

Proof 1.1 ((1)→(2)) *Suppose $s > 0$ and $\mathbf{x}^*$ is the optimal solution of (1). We have the Lagrangian of (1) with Lagrangian Multiplier $\beta \geq 0$*

$$\mathcal{L}(\beta, \mathbf{x}) = f(\mathbf{x}) + \beta(g(\mathbf{x}) - s) \tag{3}$$

By the difinition of Lagrangian dual problem, β^* is optimal for

$$\max_{\beta\geq 0} \min_{\mathbf{x}} \mathcal{L}(\beta, \mathbf{x}) = f(\mathbf{x}) + \beta(g(\mathbf{x}) - s) \tag{4}$$

The assumption of strong duality gives rise to

$$\max_{\beta\geq 0} \min_{\mathbf{x}} \mathcal{L}(\beta, \mathbf{x}) = \min_{\mathbf{x}} \max_{\beta\geq 0} \mathcal{L}(\beta, \mathbf{x}) \tag{5}$$

Submitted to 36th Conference on Neural Information Processing Systems (NeurIPS 2022). Do not distribute.

$\mathbf{x}^*$ *is the optimal solution of the saddle point problem when* β *reaches optimal*

$$\begin{aligned}\mathbf{x}^* &= \arg\min_{\mathbf{x}} \max_{\beta \geq 0} \mathcal{L}(\beta, \mathbf{x}) = f(\mathbf{x}) + \beta(g(\mathbf{x}) - s) \\ &= \arg\min_{\mathbf{x}} \mathcal{L}(\mathbf{x}) = f(\mathbf{x}) + \beta^*(g(\mathbf{x}) - s) \\ &= \arg\min_{\mathbf{x}} \mathcal{L}(\mathbf{x}) = f(\mathbf{x}) + \beta^* g(\mathbf{x})\end{aligned} \tag{6}$$

Therefore, $\mathbf{x}^*$ *is optimal for both (1) and (2) when* $\beta = \beta^*$.

Proof 1.2 ((2)→(1)) *Suppose* $\beta > 0$ *and* $\mathbf{x}^*$ *is the optimal solution of (2). We want to show* $\mathbf{x}^*$ *is also optimal for (1). Let* $s = g(\mathbf{x}^*)$. *If there exist an optimal solution* $\hat{\mathbf{x}} \neq \mathbf{x}^*$ *for (1) such that* $g(\hat{\mathbf{x}}) \leq s$, *we have*

$$\begin{aligned} & f(\hat{\mathbf{x}}) < f(\mathbf{x}^*) \\ \Rightarrow\ & f(\hat{\mathbf{x}}) + \beta g(\hat{\mathbf{x}}) < f(\mathbf{x}^*) + \beta s \\ \Rightarrow\ & f(\hat{\mathbf{x}}) + \beta g(\hat{\mathbf{x}}) < f(\mathbf{x}^*) + \beta g(\mathbf{x}^*), \end{aligned} \tag{7}$$

which contradicts that $\mathbf{x}^*$ *is optimal for (2).*

2 Convergence Analysis

The proof of ADAM in the original paper [7] is found incomplete by several works [18, 16]. A failure case of ADAM is found in [16], caused by the exponential moving average. Bock *et al.* [1] prove the local convergence in batch mode on a fixed training set. In our case, since we are optimizing over image rather than network parameters, the assumption of deterministic training set holds. Ward *et al.* [17] show the standard convergence rate of ADAM for a non-convex problem is $O(\ln(N)/\sqrt{N})$ with a scalar stepsize. Zou *et al.* [18] show that the sufficient conditions of ADAM's convergence are an appropriate initial learning rate $1/\sqrt{N}$ and exponential moving average scale $\beta_2 = 1 - 1/N$, given N the number of steps. Défossez *et al.* [3] give a simplified proof leading to the same convergence rate and conditions and extend the best known bound of ADAM from $O((1-\beta_1)^{-5})$ to $O((1-\beta_1)^{-1})$. The sign function used in previous works of adversarial attacks [8, 5] does not affect the convergence if we consider it as a fixed updating rate λ. The clamping operation restricting perturbation scale δ and box constraint within $[0, 1]$ may confine the convergence but it is necessary for optimization settings.

3 More attack results

We show more results of attack on test sets in the section. In Table 1, the detection performance gain of different attack methods for Faster-RCNN [15] is given. We can find that our method shows higher mAP boost than TOG [2]. We further give more visualization results of detection in Figure 1, 2 for hazy dataset RTTS [9] and Figure 3, 4 for low ligh dataset ExDark [12].

Table 1: The detection performance gain by different targeted adversarial attack methods on Faster-RCNN [15]. $\delta = 2/255$ and $\lambda = 1/255$.

	RTTS			VOC_fog_test			VOC_clean_test		
	no attack	TOG [2]	Ours	no attack	TOG [2]	Ours	no attack	TOG [2]	Ours
bicycle	27.15	48.38	**55.65**	44.82	82.46	**86.49**	76.34	87.78	**91.22**
bus	12.70	38.76	**48.26**	54.37	91.37	**94.59**	82.24	95.52	**97.45**
car	31.29	44.46	**47.52**	61.32	85.79	**88.99**	81.83	91.00	**93.29**
motorcycle	16.90	46.28	**50.14**	36.28	80.92	**87.27**	73.47	87.03	**90.77**
person	58.55	67.24	**70.31**	52.24	83.16	**86.03**	76.58	86.33	**88.97**
mAP	29.32	49.02	**54.37**	49.81	84.74	**88.67**	78.09	89.53	**92.34**
	ExDark			VOC_dark_test			VOC_clean_test		
	no_attack	TOG [2]	Ours	no_attack	TOG [2]	Ours	no_attack	TOG [2]	Ours
bicycle	44.71	73.09	**78.72**	57.20	79.23	**83.1**	76.61	83.83	**87.79**
boat	31.79	66.8	**75.68**	49.45	75.90	**83.58**	62.98	82.58	**86.74**
bottle	42.29	64.17	**70.56**	38.95	61.92	**68.94**	52.41	69.83	**75.76**
bus	50.65	87.59	**88.68**	64.53	85.11	**92.01**	78.62	90.82	**94.07**
car	38.58	62.71	**68.94**	67.48	82.27	**86.91**	81.71	88.80	**90.96**
cat	41.38	78.97	**83.74**	68.72	87.83	**92.31**	86.08	94.83	**97.74**
chair	35.06	77.14	**82.62**	29.84	64.23	**74.90**	49.94	74.64	**84.14**
dog	46.70	85.98	**91.01**	61.34	90.01	**95.05**	80.43	93.73	**97.81**
motorbike	27.76	54.55	**62.76**	65.04	79.93	**86.52**	75.71	85.93	**89.30**
person	40.21	62.60	**68.68**	61.14	75.87	**81.28**	77.48	84.19	**86.64**
mAP	39.91	71.36	**77.14**	56.37	78.23	**84.46**	72.20	84.92	**89.09**

(a) No attack (b) TOG [2] (c) Ours (d) No attack (e) TOG [2] (f) Ours

Figure 1: A comparison of object detection of different adversarial attack results on RTTS [9]. The 1st and 3rd rows are the results of YOLOv3 [14] and the 2nd and 4th are those of Faster-RCNN [15].

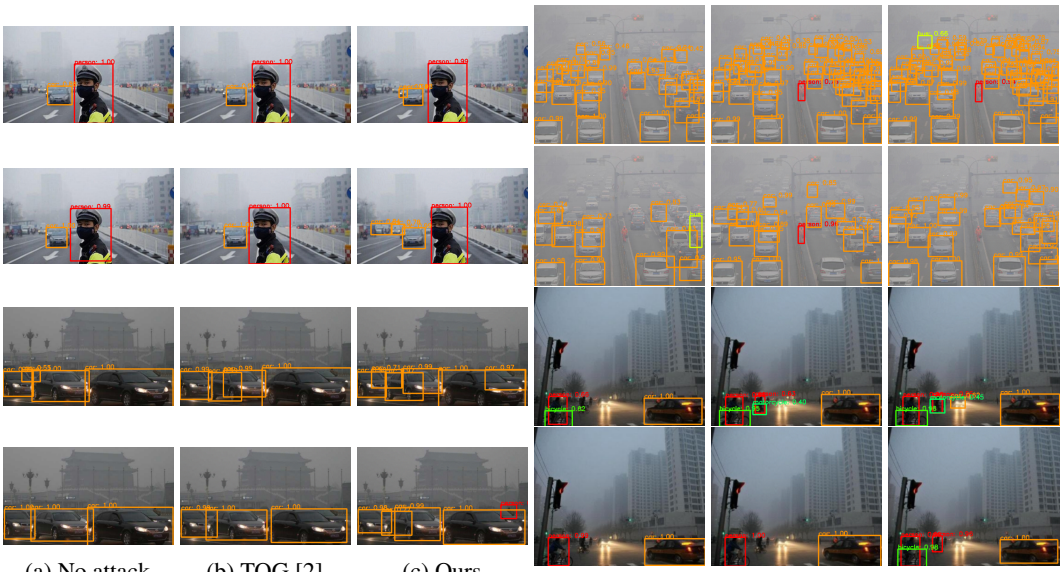

(a) No attack (b) TOG [2] (c) Ours (d) No attack (e) TOG [2] (f) Ours

Figure 2: A comparison of object detection of different adversarial attack results on RTTS [9]. The 1st and 3rd rows are the results of YOLOv3 [14] and the 2nd and 4th are thoce of Faster-RCNN [15].

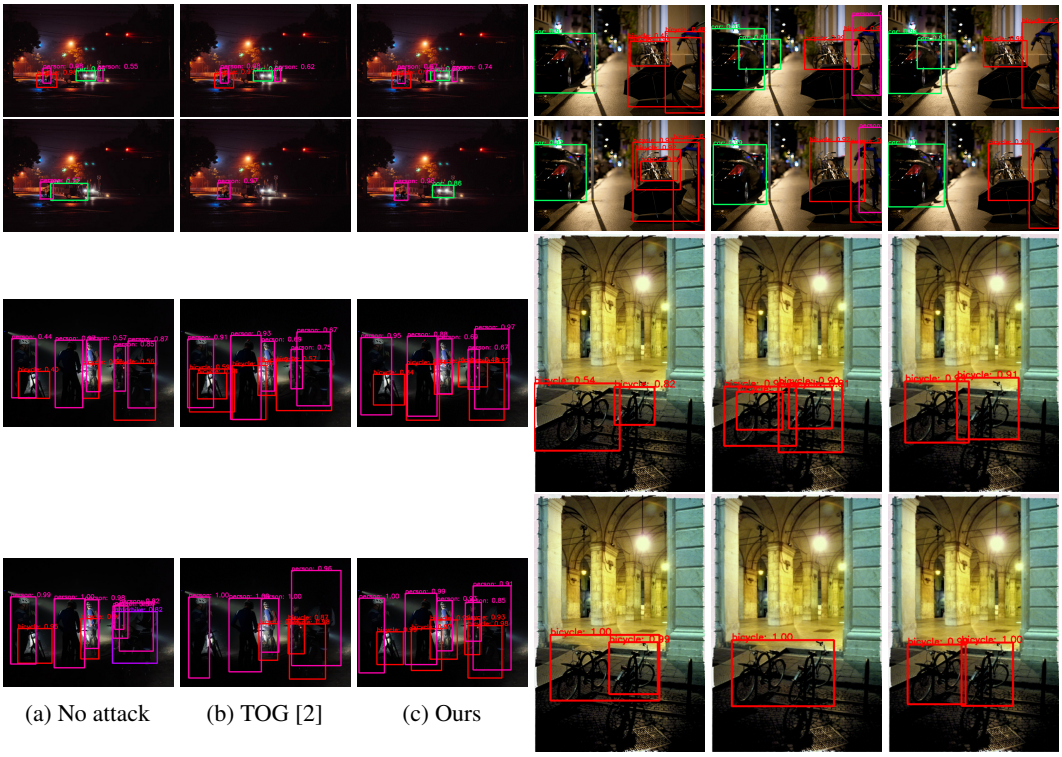

(a) No attack (b) TOG [2] (c) Ours

(d) No attack (e) TOG [2] (f) Ours

Figure 3: A comparison of object detection of different adversarial attack results on exdark [9]. The 1st and 3rd rows are the results of YOLOv3 [14] and the 2nd and 4th are those of Faster-RCNN [15].

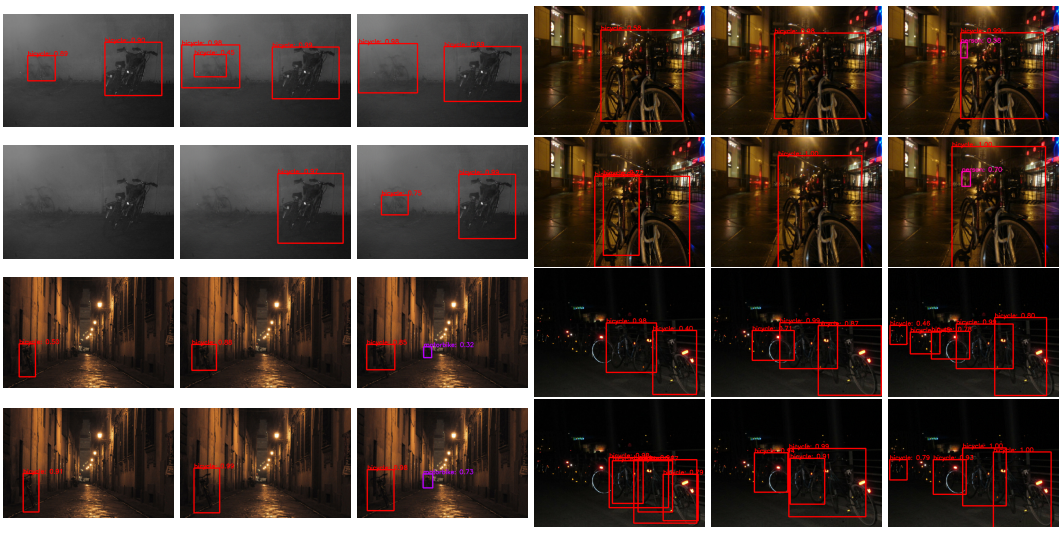

(a) No attack (b) TOG [2] (c) Ours

(d) No attack (e) TOG [2] (f) Ours

Figure 4: A comparison of object detection of different adversarial attack results on exdark [9]. The 1st and 3rd rows are the results of YOLOv3 [14] and the 2nd and 4th are those of Faster-RCNN [15].

4 More results on restoration for detection

The restoration and detection performance for Faster-RCNN [15] is shown ins Table 2 and Table 3. Several more examples for detection and restoration performance are shown in Figure 5 8.

Table 2: The quantitative results of existing methods and ours with both restoration metrics and detection metrics on VOC_fog_test and RTTS. CT refers to conventional training. F denotes Faster-RCNN [15].

		F	MSBDN			GridDehaze		
		No restoration	F+CT	F+TOG	F+Ours	F+CT	F+TOG	F+Ours
	mAP	48.58	73.67	74.30	74.62	75.12	75.45	75.49
\vocfogtest	PSNR	13.50	28.72	27.78	27.87	27.42	27.07	27.04
	SSIM	0.5411	0.8852	0.8728	0.8762	0.8667	0.8625	0.8634
RTTS	mAP	29.32	30.10	31.06	31.12	30.18	30.22	30.29

Table 3: The quantitative results of existing methods and ours with both restoration metrics and detection metrics on VOC_dark_test and ExDark. CT refers to conventional training. F denotes Faster-RCNN [15].

		F	SCI			ZeroDCE		
		No restoration	F+CT	F+TOG	F+Ours	F+CT	F+TOG	F+Ours
	mAP	56.37	59.89	60.12	60.21	59.77	60.03	60.06
\vocdarktest	PSNR	11.99	13.44	13.16	13.31	18.23	17.90	17.87
	SSIM	0.3923	0.4891	0.4791	0.4803	0.6350	0.6362	0.6357
ExDark	mAP	39.91	42.20	42.38	42.34	40.47	41.18	41.32

(a) No restoration (b) [10] (c) [4] (d) [4]+Ours (e) [11] (f) [11]+Ours

Figure 5: A comparison of object detection of different adversarial attack results on RTTS [9]. The last four columns perform detection by YOLOv3[14].

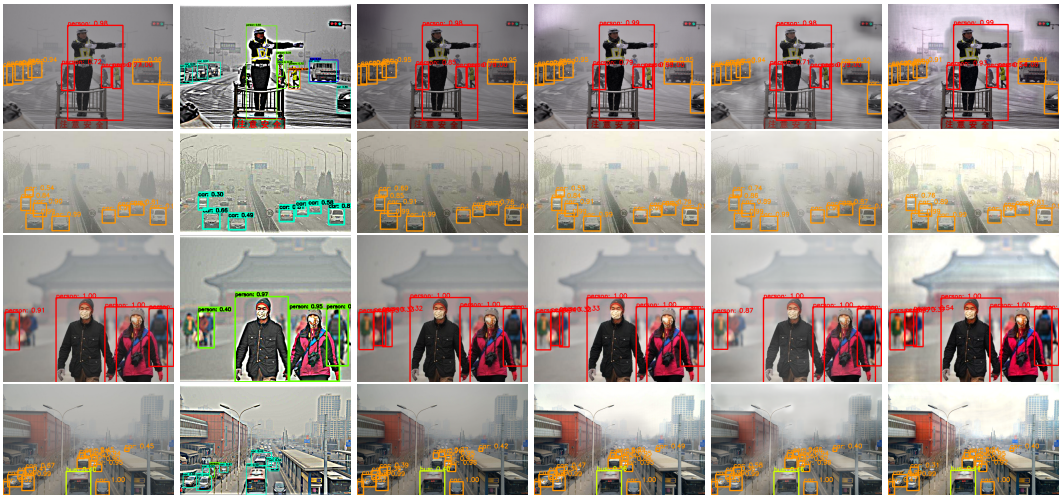

(a) No restoration (b) [10] (c) [4] (d) [4]+Ours (e) [11] (f) [11]+Ours

Figure 6: A comparison of object detection of different adversarial attack results on RTTS [9]. The last four columns perform detection by Faster-RCNN [**?**].

(a) No restoration (b) [10] (c) [6] (d) [6]+Ours (e) [13] (f) [13]+Ours

Figure 7: A comparison of object detection of different adversarial attack results on ExDark [9]. The last four columns perform detection by YOLOv3[14].

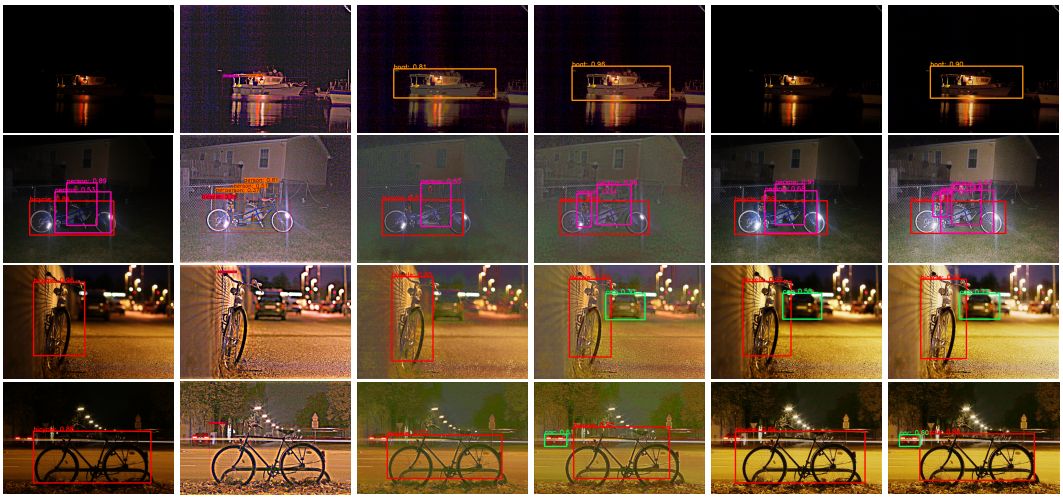

(a) No restoration (b) [10] (c) [6] (d) [6]+Ours (e) [13] (f) [13]+Ours

Figure 8: A comparison of object detection of different adversarial attack results on ExDark [9]. The last four columns perform detection by Faster-RCNN[15].

5 Statistics of Datasets

The statistics of the used datasets are provided in Table 4 and Table 5. Since there are 5 categories in dehazing datasets and low light enhancement datasets respectively, we train YOLOv3 [14] and Faster-RCNN [15] with 5 classes on VOC_fog_train and 10 classes on vocdarktrain respectively.

Table 4: The statistics of VOC_fog_train [10], VOC_fog_test [10] and RTTS [9]

	image	person	bicycle	car	bus	motorcycle	total
VOC_fog_train	8111	13256	1064	3267	822	1052	19561
VOC_fog_test	2734	4528	337	1201	213	325	6604
RTTS	4322	7950	534	18413	1838	862	29577

Table 5: The statistics of VOC_dark_train [10], VOC_dark_test [10] and ExDark [12]

	image	person	bicycle	car	bus	motorbike	boat	bottle	cat	chair	dog	total
VOC_dark_train	12334	13256	1064	3267	822	1052	1140	1764	1593	3152	2025	29135
VOC_dark_test	3760	4528	337	1201	213	325	263	469	358	756	489	8939
ExDark	2563	2235	418	919	164	242	515	433	425	609	490	6450

References

[1] Sebastian Bock and Martin Weiß. A proof of local convergence for the adam optimizer. In *2019 International Joint Conference on Neural Networks (IJCNN)*, pages 1–8, 2019.

[2] Ka-Ho Chow, Ling Liu, Margaret Loper, Juhyun Bae, Mehmet Emre Gursoy, Stacey Truex, Wenqi Wei, and Yanzhao Wu. Adversarial objectness gradient attacks in real-time object detection systems. In *2020 Second IEEE International Conference on Trust, Privacy and Security in Intelligent Systems and Applications (TPS-ISA)*, pages 263–272, 2020.

[3] Alexandre Défossez, Léon Bottou, Francis Bach, and Nicolas Usunier. A simple convergence proof of adam and adagrad. *arXiv preprint arXiv:2003.02395*, 2020.

[4] Hang Dong, Jinshan Pan, Lei Xiang, Zhe Hu, Xinyi Zhang, Fei Wang, and Ming-Hsuan Yang. Multi-scale boosted dehazing network with dense feature fusion. In *2020 IEEE/CVF Conference on Computer Vision and Pattern Recognition (CVPR)*, pages 2154–2164, 2020.

[5] Yinpeng Dong, Fangzhou Liao, Tianyu Pang, Xiaolin Hu, and Jun Zhu. Discovering adversarial examples with momentum. *arXiv preprint arXiv:1710.06081*, 2017.

[6] Chunle Guo, Chongyi Li, Jichang Guo, Chen Change Loy, Junhui Hou, Sam Kwong, and Runmin Cong. Zero-reference deep curve estimation for low-light image enhancement. In *2020 IEEE/CVF Conference on Computer Vision and Pattern Recognition (CVPR)*, pages 1777–1786, 2020.

[7] Diederik P Kingma and Jimmy Ba. Adam: A method for stochastic optimization. *arXiv preprint arXiv:1412.6980*, 2014.

[8] Alexey Kurakin, Ian J. Goodfellow, and Samy Bengio. Adversarial examples in the physical world. *ArXiv*, abs/1607.02533, 2017.

[9] Boyi Li, Wenqi Ren, Dengpan Fu, Dacheng Tao, Dan Feng, Wenjun Zeng, and Zhangyang Wang. Benchmarking single-image dehazing and beyond. *IEEE Transactions on Image Processing*, 28(1):492–505, 2019.

[10] Wenyu Liu, Gaofeng Ren, Runsheng Yu, Shi Guo, Jianke Zhu, and Lei Zhang. Image-adaptive yolo for object detection in adverse weather conditions. In *Proceedings of the AAAI Conference on Artificial Intelligence*, 2022.

[11] Xiaohong Liu, Yongrui Ma, Zhihao Shi, and Jun Chen. Griddehazenet: Attention-based multi-scale network for image dehazing. In *2019 IEEE/CVF International Conference on Computer Vision (ICCV)*, pages 7313–7322, 2019.

[12] Yuen Peng Loh and Chee Seng Chan. Getting to know low-light images with the exclusively dark dataset. *Computer Vision and Image Understanding*, 178:30–42, 2019.

[13] Long Ma, Tengyu Ma, Risheng Liu, Xin Fan, and Zhongxuan Luo. Toward fast, flexible, and robust low-light image enhancement. *CoRR*, abs/2204.10137, 2022.

[14] Joseph Redmon and Ali Farhadi. Yolov3: An incremental improvement. *CoRR*, abs/1804.02767, 2018.

[15] Shaoqing Ren, Kaiming He, Ross Girshick, and Jian Sun. Faster r-cnn: Towards real-time object detection with region proposal networks. *IEEE Transactions on Pattern Analysis and Machine Intelligence*, 39(6):1137–1149, 2017.

[16] J REDDI Sashank, Kale Satyen, and Kumar Sanjiv. On the convergence of adam and beyond. In *International Conference on Learning Representations*, volume 5, page 7, 2018.

[17] Rachel Ward, Xiaoxia Wu, and Leon Bottou. Adagrad stepsizes: Sharp convergence over nonconvex landscapes. In *International Conference on Machine Learning*, pages 6677–6686. PMLR, 2019.

[18] Fangyu Zou, Li Shen, Zequn Jie, Weizhong Zhang, and Wei Liu. A sufficient condition for convergences of adam and rmsprop. In *Proceedings of the IEEE/CVF Conference on Computer Vision and Pattern Recognition*, pages 11127–11135, 2019.